Journal of Applied Polymer Science

Sensing and surface morphological properties of a poly[(9,9-dioctylfluorenyl-2,7-diyl)-*co*-bithiophene] liquid-crystalline polymer for optoelectronic applications

Bayram Gündüz
Department of Science Education, Faculty of Education, Muş Alparslan University, Muş 49250 Turkey
Correspondence to: B. Gunduz (E-mail: bgunduz83@hotmail.com or b.gunduz@alparslan.edu.tr)

ABSTRACT: The sensing properties of a poly[(9,9-dioctylfluorenyl-2,7-diyl)-*co*-bithiophene] (F8T2) polymer were investigated at different concentrations and volume percentages. The effects of the concentrations and volume percentages on the sensing parameters were investigated. The sensitivities of F8T2 were found to be 3.190, 1.434, and 0.362 dB/vol % at 290, 580, and 940 nm, respectively. The response of the F8T2 increased with increasing concentration. F8T2 exhibited good sensitivity and response behaviors. Then, the optical parameters based on the refractive indices of the F8T2 at different molarities were calculated. The dispersion energy, moment of the dielectric constant optical spectrum (M_{-1}, M_{-3}), oscillator strength, and contrast of the F8T2 increased with increasing molarity, whereas the average excitation energy or single-oscillator energy decreased with increasing molarity. The surface morphological properties of the F8T2 polymer film were investigated, and the roughness parameters were obtained. The F8T2 polymer could be used in the fabrication of various sensors because of the good solubility, sensitivity, and response behaviors. © 2014 Wiley Periodicals, Inc. J. Appl. Polym. Sci. **2015**, *132*, 41659.

KEYWORDS: morphology; nanostructured polymers; optical and photovoltaic applications; optical properties; sensors and actuators

Received 27 August 2014; accepted 20 October 2014
DOI: 10.1002/app.41659

INTRODUCTION

Organic materials have recently obtained considerable attention because of their facile and large-scale synthesis,[1] flexibility,[2] low-cost manufacturing,[3] potential in large areas and light weight,[4] easy processing,[5] attractive mechanical and chemical properties,[6] interesting sensing properties[7] or high luminescence[7] and photoluminescence efficiency,[6] high versatility in molecular energetics and the crystal structure,[8] optoelectronic properties,[6] high absorption coefficients,[9] good and solution processability,[1] molecular and electronic tunability by molecular design,[10] fundamental importance in understanding of intermolecular interactions,[11] and for many components of electronic devices in many electronic, optical, optoelectronic, and photonic applications,[7] such as electronic displays,[12,13] color tunable displays,[14] solar cells,[4,5,9] photovoltaics,[5] electroluminescent diodes,[15] light-emitting diodes,[5,7,13] smart cards,[13] memory elements,[16] radio-frequency identification tags,[17] optoelectronic devices,[4,13] optical waveguides,[18] thin-film transistors,[19] field-effect transistors,[7,17,20] phototransistors,[17] photodetectors,[21] thermoelectric generators,[22] lasers,[23] nanoscale lasers,[24] sensors,[25] gas sensors,[26,27] and chemical sensors,[28] over their inorganic counterparts. These widely significant devices and applications can be achieved through an understanding of the fundamental and important properties, such as the electrical, photoelectrical, photovoltaic, optical, sensing, and surface morphological properties of the organic materials/semiconductors. Organic semiconductors are significant materials because their processing conditions are much lighter than those used to make amorphous and crystalline inorganic semiconductors.

Fluorene-type polymers are significant conducting polymers because of their high mobility, efficient emission, high stabilities, and full color emission.[29] Poly(9,9-dioctylfluorene) contains only a fluorene backbone, and it exhibits various morphological behaviors and blue emission features.[29] Poly[(9,9-dioctylfluorenyl-2,7-diyl)-*co*-bithiophene] (F8T2) is a liquid-crystalline polymer and is a promising material for electronic and optoelectronic[30] applications because the F8T2 polymer indicates a good stability, high field-effect mobility,[30] good thermotropic liquid crystallinity,[31] and excelent hole-transporting properties.[32]

Sensors are very significant electronic circuit components; they make our daily lives easier, and they have an important role in personal and national security, environmental sensing, biochemical sensing, energy conservation, industrial manufacturing, and many sectors, such as agriculture, medicine, automotive, and space industry.[33] There are various sensors, including optical sensors, chemical sensors, electrochemical sensors, optical

chemical sensors, optical fiber sensors, fiber-optic sensors, fiber-optic chemical sensors, evanescent field absorption fiber sensors, fiber-based refractive index (RI or *n*) sensors, fiber-optic RI sensors, luminescent sensors, evanescent wave sensors, ultraviolet sensors, speed sensors, humidity sensors, gas sensors, biosensors, magnetic field sensors, pressure sensors, temperature sensors, and vibration sensors.[18,25,27,33–38]

The use of conducting polymers and organic semiconductors in chemical sensors has received much interest thanks to their sensing properties. The sensitive parameters for chemical sensors can be changed with the conductivity, work function, and optical absorption coefficient of the materials.[39] The optical properties of the materials affect the sensitive parameters of chemical sensors. F8T2 can be used to improve device performance and sensing and surface morphological properties.

Similarly, the surface roughness parameters affect the fundamental properties of many electronic, optoelectronic, and photonic applications, such as solar cells, photovoltaics, light-emitting diodes, electroluminescent diodes, transistors, smart cards, radio-frequency identification tags, photodetectors, lasers, optical waveguides and displays, and sensors. For this reason, the surface roughness parameters of organic semiconductor films are significant in the investigation of the surface morphological properties, and they can be obtained from an atomic force microscopy (AFM) device. The surface roughness parameters of semiconductor films affect the performances of sensor design, biological imaging, light-emitting devices, and detection.[40] The surface morphological properties of the materials can affect the luminescence and charge-transport properties.[41]

Furthermore, many scientists have done many studies on the sensing and surface properties of various materials for optoelectronic and sensor applications. Mitsushio *et al.*[42] reported that the response values of surface plasmon resonance (SPR) optical fiber sensors increased with decreasing refractivities and with increasing film thicknesses. Lalova and Todorov[43] investigated the optical properties of porous chalcogenide films for sensor applications. They varied the RI from 1.78 to 2.42 at 1550 nm. Politakos *et al.*[44] studied the optical and surface properties of a polystyrene-*b*-poly(thiophene) copolymer doped with fullerenes. Exley[45] investigated the optical properties of novel phthalocyanine compounds for sensor devices. Echabaane *et al.*[3] investigated the optical and sensing properties of β-ketoimine calix[4]arene thin films. Ates *et al.*[33] studied humidity sensors, analyzed their surface properties with AFM, and obtained many optical parameters, including the optical band gap and absorption coefficient for undoped and Sn doped ZnO metal oxide semiconductors. Faisal *et al.*[46] evaluated the sensing properties of CuO nanosheets. Rossberg[47] obtained important optical parameters, such as the reflection, RI, free carrier density, transmission, and absorption coefficient for sensors. Chen *et al.*[36] investigated the humidity-sensing properties of gold–poly(vinyl pyrrolidone) core–shell nanocomposites. Armin *et al.*[48] investigated the absorption coefficients based on the concentration without fiber-optic sensors and by fiber-optic sensors. They reported that the free-beam and evanescent field absorption coefficients increased with increasing concentration. Acar *et al.*[34] investigated the humidity-sensing properties of conducting polypyrrole/polyacrylonitrile composite fibers. Manera *et al.*[49] determined the optical parameters of colloidal TiO_2 nanocrystal-based thin films for sensing applications. Kumar *et al.*[50] studied the surface morphological and optical properties of the nanodimensional self-assembly of regioregular poly(3-hexylthiophene). Purniawan *et al.*[18] found the contrast ($\alpha_c = 0.7$), RI ratio (1.8), and sensitivities (0.85 and 1.34 dB/vol %, respectively) for ethanol and isopropyl alcohol. Adhyapak *et al.*[51] studied the optical humidity-sensing properties of cobalt/poly(vinyl alcohol) nanocomposites.

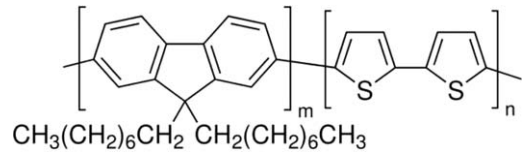

Figure 1. Chemical structure of the F8T2 liquid-crystalline polymer.

In this study, optical parameters based on the RI of the F8T2 polymer were calculated at 1.200 and 2.290 μM. Then, the sensing properties of the F8T2 polymer were investigated at 0.987, 1.883, 2.813, 4.046, and 7.780 mg/L concentrations and 0.121, 0.230, 0.343, 0.494, and 0.950 vol % volume percentages. The effects of the concentrations and volume percentages on the sensing parameters of the F8T2 liquid-crystalline polymer were investigated. I could not find any reports on the surface roughness parameters of only the F8T2 polymer film in the literature. For this reason, the surface morphological properties of the F8T2 film were studied by high-performance AFM, and the surface roughness parameters of the F8T2 film were obtained. Finally, the possibility of using these parameters for optoelectronic applications is discussed, and this study is compared with similar and related studies in the literature.

EXPERIMENTAL

The F8T2 liquid-crystalline polymer and solvents used in this study were purchased from Sigma–Aldrich Co. The chemical structure of the F8T2 polymer is depicted in Figure 1. This section occurred in three stages. First, the stock solutions of the F8T2 liquid-crystalline polymer were prepared at different molarities, concentrations, and volume percentages. Then, optical measurements of the solutions of the F8T2 polymer were recorded at different molarities, concentrations, and volume percentages. In the last stage, the F8T2 film for AFM at 16.447 μM was prepared.

Preparation of the Solutions of the F8T2 Polymer at Different Molarities, Concentrations, and Volume Percentages

First, the F8T2 polymer was weighed with an AND-GR-200 series analytical balance at 1.200 and 2.290 μM molarities; 0.987, 1.883, 2.813, 4.046, and 7.780 mg/L concentrations; and 0.121, 0.230, 0.343, 0.494, and 0.950 vol %. Then, these weighed F8T2 polymers were dissolved homogeneously in 8 mL of toluene solvent.

Optical Measurements of the F8T2 Polymer at Different Molarities, Concentrations, and Volume Percentages

Cylindrical cuvettes (Hellma QS-100) 3.5 mL in volume and 10 mm in optical path length were used for all of the solutions of the F8T2 polymer. The optical measurements of all of the solutions of the F8T2 polymer at different molarities,

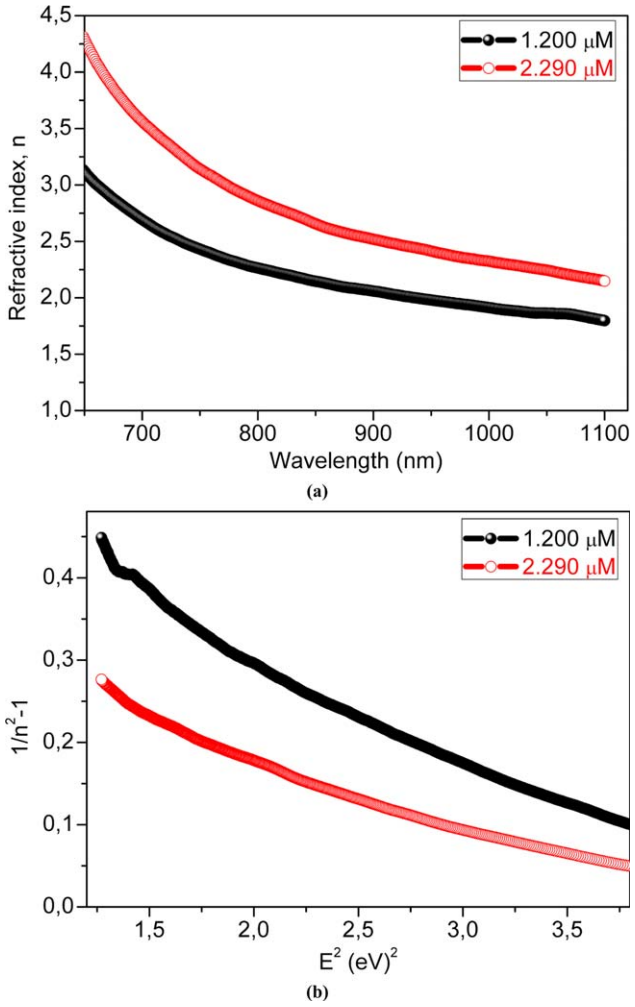

Figure 2. Plots of (a) n versus λ and (b) $1/(n^2-1)$ versus E^2 for the F8T2 polymer at 1.200 and 2.290 μM. [Color figure can be viewed in the online issue, which is available at wileyonlinelibrary.com.]

concentrations, and volume percentages were recorded with a Shimadzu model UV-1800 spectrophotometer at wavelengths of 1100–190 nm at room temperature.

Preparation of the F8T2 Films for Surface Morphology

To prepare the F8T2 films, the F8T2 material was weighed with an AND-GR-200 series analytical balance at 16.447 μM. Then, it was dissolved homogeneously in 10 mL of chloroform and filtered through polytetrafluoroethylene membrane filter to obtain a better film. Ultimately, the solution of the F8T2 filtered was coated on cleaned microscopy glass. After coating, the film was dried at 80°C for 10 min to evaporate the solvent and remove organic residuals. The surface morphological properties of the F8T2 film were studied by high-performance AFM (NanoMagnetics Instruments Co.) with a PPP-XYNCHR-type cantilever in dynamic mode.

RESULTS AND DISCUSSION

Here, the optical parameters based on the RIs of the F8T2 polymer were calculated. Then, the sensing properties of the F8T2 liquid-crystalline polymer were investigated at different concentrations and volume percentages. Finally, the surface morphological properties of the F8T2 film were studied.

Optical Parameters Based on the RIs of the F8T2 Polymer at Different Molarities

RI (n) is a significant fundamental parameter for electronic and optoelectronic applications. The optical properties of a material can be characterized by its RI. The RI obtained from the following equation:[52–54]

$$n=\left\{\left[\frac{4R}{(R-1)^2}-k^2\right]^{1/2}-\frac{R+1}{R-1}\right\} \quad (1)$$

where R is the reflectance and k is the extinction coefficient. The n values of the F8T2 polymer at 1.200 and 2.290 μM were obtained from eq. (1). Figure 2(a) indicates the plot of n versus wavelength (λ) of the F8T2 polymer at 1.200 and 2.290 μM. As shown Figure 2(a), the RI of the F8T2 polymer decreased with decreasing molarity and increasing photon energy (E). The n values for 1.200 μM varied from 3.122 to 1.797, whereas the RI (n) values for 2.290 μM varied from 4.290 to 2.149.

In normal dispersion region, the RI dispersion was analyzed with the single-oscillator model, whereas in the abnormal (anomalous) dispersion region, the RI was analyzed with a multioscillator model.[55] The dispersion of the RI is given with the well known Wemple–DiDomenico equation as follows:[52–54,56,57]

$$n^2-1=\frac{E_dE_o}{E_o^2-E^2} \quad (2)$$

where E_d is the dispersion energy and is a measure of the strength of interband optical transitions and E_0 is the average excitation energy or single-oscillator energy for electronic transitions. The experimental verification of eq. (2) can be obtained through a plot of $(n^2-1)^{-1}$ versus square (E^2) of photon energy. The resulting straight line yields the E_0 and E_d parameters. The plot of the $1/(n^2-1)$ versus E^2 of the F8T2 polymer for 1.200 and 2.290 μM is shown in Figure 2(b). The E_0 and E_d values of the solutions of the F8T2 polymer for 1.200 and 2.290 μM were obtained and are given in Table I. As shown in Table I, the E_d value (4.196 eV) of the F8T2 polymer for 1.200 μM was lower than the E_d value (6.692 eV) of the F8T2 polymer at 2.290 μM, whereas the E_0 value (2.147 eV) of the F8T2 polymer at 1.200 μM was higher than the E_0 value (2.135 eV) of the F8T2 polymer at 2.290 μM. The E_d values (4.196 and 6.692 eV) of the F8T2 polymer were lower than the E_d value (14.532 eV) of the CoPc thin film,[55] the E_d value (10.0 eV) of the $Y_{0.225}Sr_{0.775}CoO_{3\pm\delta}$ thin film,[58] and the E_d value (6.59 eV) of the 3,4,9,10-perylene-tetracarboxylic-diimide (PTCDI) thin film,[41] whereas the E_d value (6.692 eV) of the F8T2 polymer was higher than the E_d value (6.017 eV) of another PTCDI thin film.[59] The E_0 values (2.147 and 2.135 eV) of the F8T2 polymer were lower than the E_0 value (2.41 eV) of the first PTCDI thin film,[41] the E_0 value (2.909 eV) of the second PTCDI thin film,[59]

Table I. Optical Parameters Based on the RIs of the F8T2 Polymer at 1.200 and 2.290 μM.

Molarity (μM)	E_d (eV)	E_0 (eV)	M_{-1}	M_{-3} (eV^{-2})	f (eV^2)
1.200	4.196	2.147	1.954	0.424	9.009
2.290	6.692	2.135	3.134	0.688	14.287

the E_0 value (3.76 eV) of the $Y_{0.225}Sr_{0.775}CoO_{3\pm\delta}$ thin film,[58] and the E_0 value (5.5 eV) of the CoPc thin film[55] reported in the literature. As shown in Table I, the E_0 values of the F8T2 polymer were lower than the E_d values.

M_{-1}, M_{-3} are moment of optical spectrum and the -1, -3 moment are involved in computation of E_0 and E_d. The M_{-1} and M_{-3} moments of the F8T2 polymer were calculated as follows:[58]

$$E_0^2 = \frac{M_{-1}}{M_{-3}} \quad (3)$$

and

$$E_d^2 = \frac{M_{-1}^3}{M_{-3}}$$

The M_{-1} and M_{-3} moments of the F8T2 polymer for 1.200 and 2.290 μM were obtained and are listed in Table I. As shown in Table I, the M_{-1} and M_{-3} moment values (1.954 and 0.424 eV^{-2}, respectively) of the F8T2 polymer at 1.200 μM were lower than the M_{-1} and M_{-3} moment values (3.134 and 0.688 eV^{-2}, respectively) of the F8T2 polymer at 2.290 μM. We observed that the M_{-1} and M_{-3} moments of the F8T2 polymer increased with increasing molarity. The M_{-1} moment (1.954) of the F8T2 polymer at 1.200 μM was lower than the M_{-1} moment (2.618) of the CoPc thin film[55] and the M_{-1} moment (2.66) of the $Y_{0.225}Sr_{0.775}CoO_{3\pm\delta}$ thin film[58] reported in the literature, whereas the M_{-1} moment (3.134) of the F8T2 polymer for 2.290 μM was higher than the M_{-1} moment (2.618) of the CoPc thin film[55] and the M_{-1} moment (2.66) of another $Y_{0.225}Sr_{0.775}CoO_{3\pm\delta}$ thin film[58] in the literature. The M_{-3} moments (0.424 and 0.688 eV^{-2}) of the F8T2 polymer for 1.200 and 2.290 μM were higher than the M_{-3} moment (0.084 eV^{-2}) of the CoPc thin film[55] and the M_{-3} moment (0.19 eV^{-2}) of the $Y_{0.225}Sr_{0.775}CoO_{3\pm\delta}$ thin film[58] in the literature.

For optical transitions, the optical oscillator strengths (f's) are considered as the absorption of a photon by the electron between the initial state and the final state.[58] The transition rate is proportional to the square of f (f^2). Thus, f may be regarded as an indicator of how strongly the materials interact with the radiation. Therefore, f is a significant parameter, and it is calculated with the following equation:[56]

$$f = E_0 E_d \quad (4)$$

The f values of the F8T2 polymer at 1.200 and 2.290 μM were obtained and are listed in Table I. As shown in Table I, the f value (9.009 eV^2) of the F8T2 polymer for 1.200 μM was lower than the f value (14.287 eV^2) of the F8T2 polymer at 2.290 μM. The f values (9.009 and 14.287 eV^2) of the F8T2 polymer at 1.200 and 2.290 μM were lower than the f value (37.51 eV^2) of the $Y_{0.225}Sr_{0.775}CoO_{3\pm\delta}$ thin film.[58]

Sensing Properties of the F8T2 Polymer at Different Concentrations

The sensitivity (S) of a sensory materials is related to α_c, which is a normalized RI. α_c can be calculated as follows:[18]

$$\alpha_c = 1 - \left(\frac{n_1}{n_2}\right)^2 \quad (5)$$

where n_1 is the refractive index of the medium and n_2 is the refractive index of the solutions of the material. The α_c values

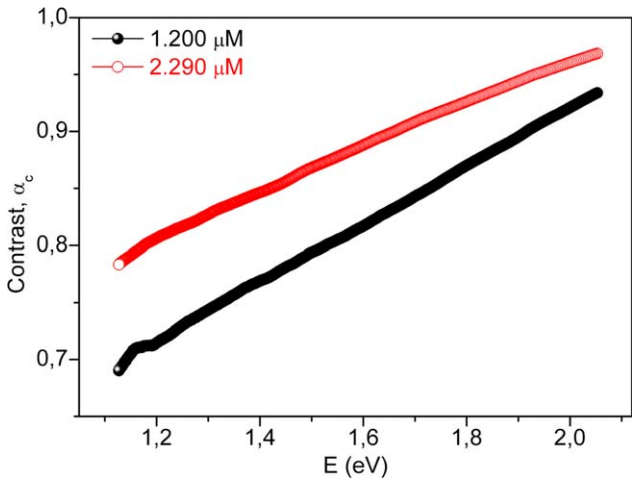

Figure 3. Plot of α_c versus E for the F8T2 polymer at 1.200 and 2.290 μM. [Color figure can be viewed in the online issue, which is available at wileyonlinelibrary.com.]

of the F8T2 polymer at 1.200 and 2.290 μM were obtained. As viewed in Figure 3, α_c of the F8T2 polymer sharply increased with increasing E and increasing molarity. The values of α_c at 1.200 and 2.290 μM were higher than 0.69 and 0.78, respectively. The α_c ($\alpha_c > 0.69$ and 0.78) and RI ratio (from 3.22 to 1.797 and from 4.290 to 2.149) values of the F8T2 polymer for 1.200 and 2.290 μM were higher the than α_c ($\alpha_c > 0.57$ and 0.7) and RI ratio (1.5 and 1.8) of a TiO_2–Atomic Layer Deposition (ALD) evanescent waveguide sensor.[18,60] This was attributed to the types of used materials, solvents, and molarity value. These results suggest that the E_d, M_{-1} and M_{-3} moments, f, and α_c of the F8T2 increased with increasing molarity, whereas E_0 decreased with increasing molarity.

The absorbance is directly dependent on the molar concentration of absorbing molecules and the optical path length. Figure 4(a,b) denotes the curves of the absorbance and transmittance (%T) versus the concentration of the solutions of the F8T2 polymer in the near-ultraviolet (at 290 nm), visible (at 580 nm), and near-infrared (at 940 nm) regions. As shown in Figure 4(a), the absorbance ($-\log_{10} T$) increased with increasing concentration, whereas %T decreases geometrically because of its logarithmic dependence (at 290 and 580 nm) on the concentration with increasing concentration [Figure 4(b)]. As shown in Figure 4(a), the absorbance decreased with the variation of the wavelength from 290 to 940 nm, whereas %T increased with the variation of the wavelength from 290 to 940 nm [Figure 4(b)].

The evanescent absorption coefficients (k_{ev}'s) of the F8T2 polymer were calculated at different wavelengths and concentrations. As shown in Figure 5, the k_{ev}'s are on the order of inverse nanometers, whereas the absorption coefficients (α) were on the order of inverse centimeters. That is, the absorption coefficients of the F8T2 polymer were higher than the k_{ev}'s of the F8T2 polymer. As shown in Figure 5, the α and k_{ev} values of the F8T2 polymer at 580 and 940 nm increased with increasing concentration, but the α and k_{ev} values at 290 nm increased until a certain concentration was reached. Then, they decreased

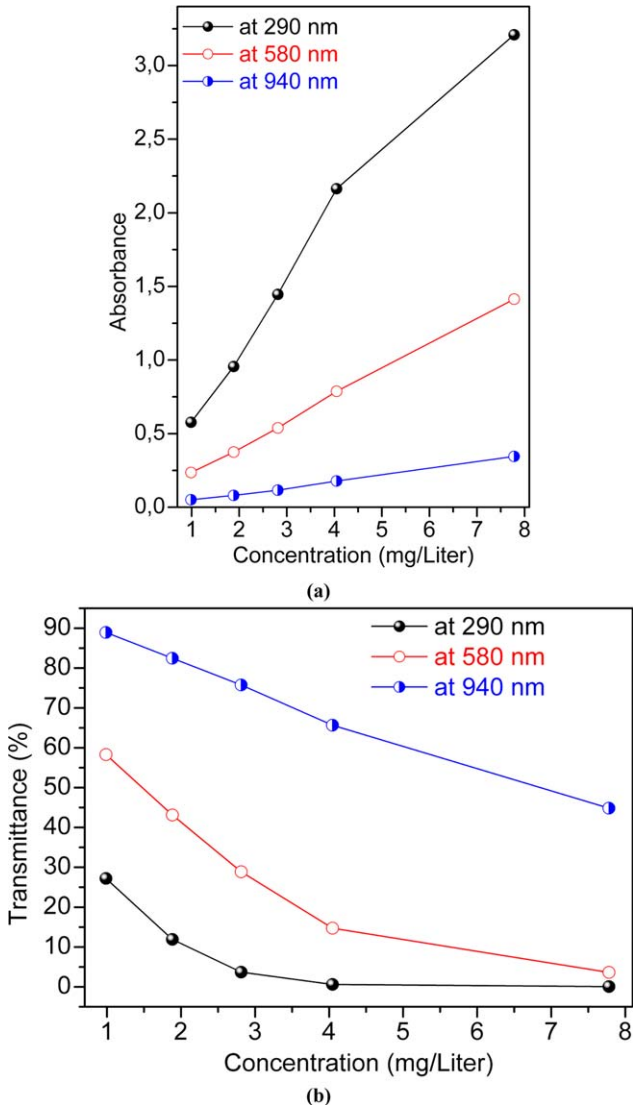

Figure 4. Curves of the (a) absorbance and (b) %T versus the concentration of solutions of the F8T2 polymer at 290, 580, and 940 nm. [Color figure can be viewed in the online issue, which is available at wileyonlinelibrary.com.]

with increasing concentration. The correlation coefficient values of the linear fitting of the F8T2 polymer at 580 and 940 nm were found to be 0.972 and 0.992, respectively. The correlation coefficient values (0.972 and 0.992) of the solution of the F8T2 molecule at 580 and 940 nm were close to the correlation coefficient values (0.96, 0.92, and 0.86) of the solutions of the methylene blue dye for various pH values[48] in the literature.

S could be obtained by the following:[18]

$$S = \frac{\Delta A}{\Delta \% V} \tag{6}$$

Figure 6 indicates the plot of the absorbance versus the volume percentage (vol % or %V) the solutions of the F8T2 polymer at 290, 580, and 940 nm. The sensitivities of the F8T2 polymer were calculated as the slopes shown in Figure 6 and were found to be 3.190, 1.434, and 0.362 dB/vol % at 290, 580, and 940 nm, respectively. We observed that the highest S (3.190

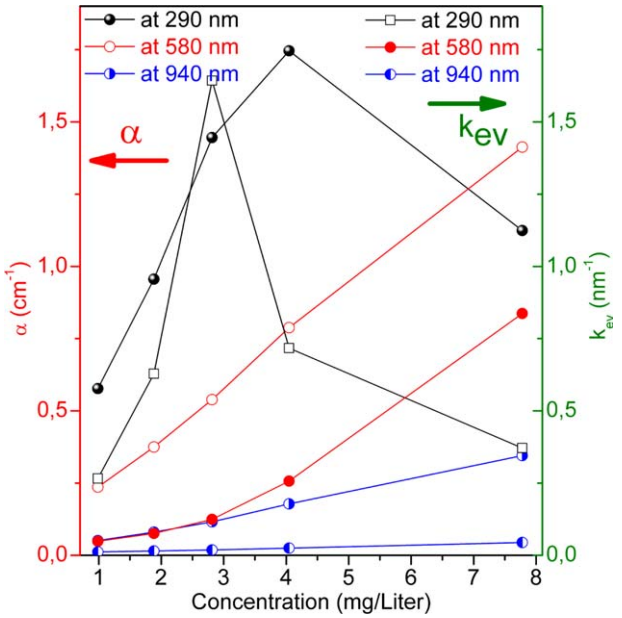

Figure 5. Plot of the absorption coefficient (α) and k_{ev} versus the concentration of the F8T2 polymer at 290, 580, and 940 nm. [Color figure can be viewed in the online issue, which is available at wileyonlinelibrary.com.]

dB/vol %) of the F8T2 polymer was obtained at 290 nm, whereas the lowest S (0.362 dB/vol %) of the F8T2 polymer was obtained at 940 nm. We observed that the F8T2 polymer exhibited good S behavior.

Response values of the F8T2 polymer at 290, 580, and 940 nm were obtained. As shown in Figure 7, the response of the F8T2 polymer increased with increasing concentration, and the

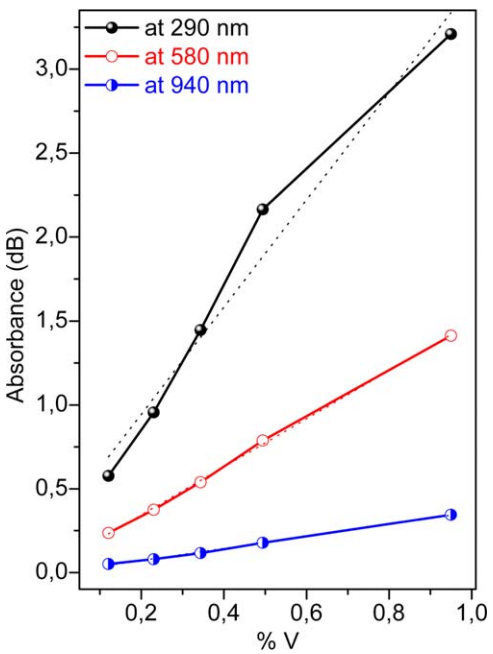

Figure 6. Plot of the absorbance versus volume percentage of the F8T2 polymer at 290, 580, and 940 nm. [Color figure can be viewed in the online issue, which is available at wileyonlinelibrary.com.]

response at 290 nm was the highest, whereas the response at 940 nm was the lowest. It was observed that the F8T2 polymer exhibited good response behavior, and the response of the F8T2 polymer changed with different concentrations and wavelengths.

Surface Morphological Properties of the F8T2 Film

The surface morphological properties of the F8T2 film were studied by high-performance AFM. Figure 8(a,b) shows one-dimensional (1D) and three-dimensional (3D) AFM topography images, respectively, of the F8T2 film for a 5 × 5 μm^2 scan area. As shown in Figure 8(a,b), the topography images had light, dark, and bumpy regions.

Here, the surface roughness parameters, such as roughness average (sa), root mean square roughness (sq), surface skewness (ssk), and surface kurtosis (sku) values of the F8T2 film, were obtained from the AFM images with an AFM software program. The sa value (3.097 nm) of the F8T2 film was lower than the sq value (3.936 nm). The sq/sa value (1.271) of the F8T2 film for the 5 × 5 μm^2 scan area was reasonably close to the value of 1.25 predicted by theory.[61] This result was significant because it indicated that at the imaging scale, the asperity height distribution of these surfaces were approximately Gaussian and that the statistical relationships for the surface roughness were applicable.[62] The surface skewness value (1.230) of the F8T2 film was a positive value; this indicated that the peaks were dominant on the surface. Surfaces with a positive skewness, such as turned surfaces, have fairly high spikes that protrude above a flatter average.[63] A positive ssk value of the F8T2 film, as shown in Figure 8(a,b), indicates a surface with islands and an asymmetry in the height histogram and an additional Gaussian component

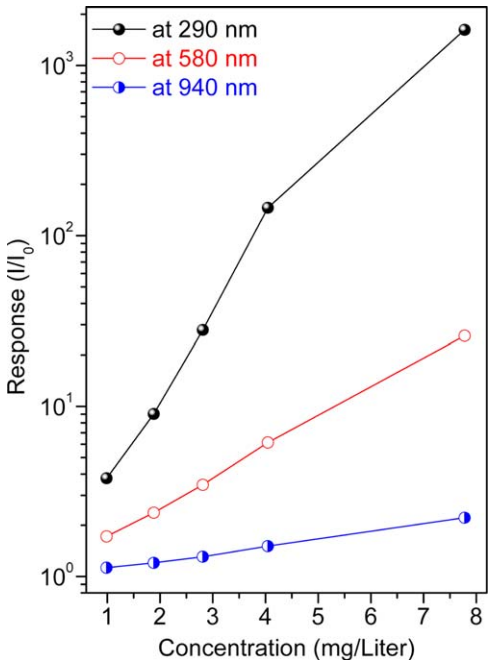

Figure 7. Plot of the response versus the concentration of the solutions of the F8T2 polymer at 290, 580, and 940 nm. I_0: the intensity of incident light on the substance of interest, I: the intensity of light leaving the substance. [Color figure can be viewed in the online issue, which is available at wileyonlinelibrary.com.]

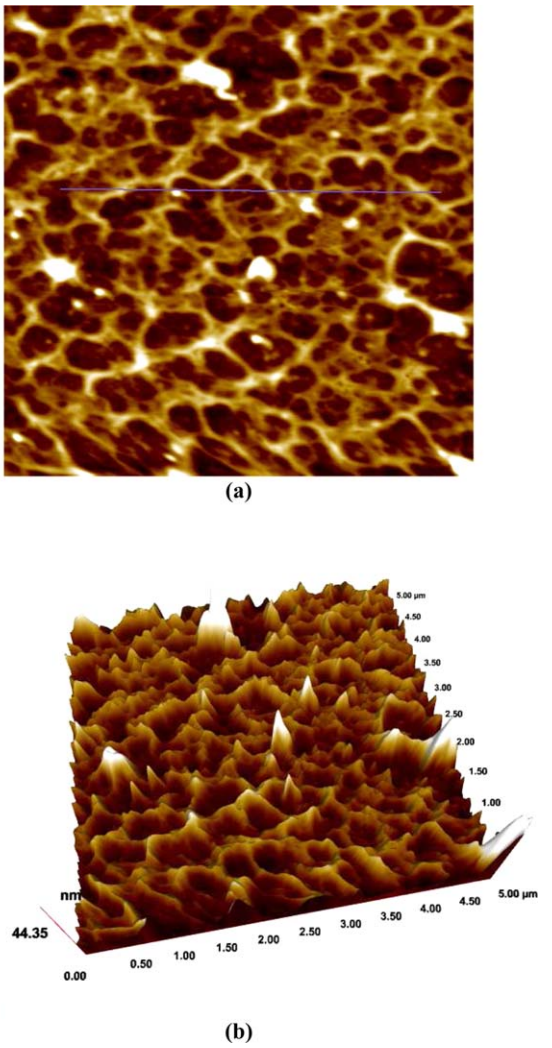

Figure 8. (a) 1D and (b) 3D AFM topography images (5 × 5 μm^2 scan area) of the F8T2 film. [Color figure can be viewed in the online issue, which is available at wileyonlinelibrary.com.]

in the height distribution (HD).[64] The surface kurtosis value (7.836) of the F8T2 film was higher than 3; this indicated low valleys with a bumpy surface, as also shown in Figure 8(a,b). The results of the sku values of the F8T2 film show that the F8T2 film indicated spiky[65] and sharp islands or holes[64] on the surfaces, as shown in Figures 8(a,b). It is known that the rough surfaces with high kurtosis and positive skewness values reduce friction.[13]

CONCLUSIONS

In this study, we obtained interesting and useful sensing results for sensor applications. The sensitivities of the F8T2 polymer were found to be 3.190, 1.434, and 0.362 dB/vol % at 290, 580, and 940 nm, respectively. The response of the F8T2 polymer increased with increasing concentration, and the response at 290 nm was the highest, whereas the response at 940 nm was the lowest. The F8T2 polymer exhibited high visible *S* and response behavior. The visible *S* and cutoff change of the response of the F8T2 polymer could be changed by different

molarities and concentrations. The n values for 1.200 μM varied from 3.122 to 1.797, whereas the RI (n) values for 2.290 μM varied from 4.290 to 2.149. The E_d value (4.196 eV) of the F8T2 polymer at 1.200 μM was lower than the E_d value (6.692 eV) of the F8T2 polymer at 2.290 μM, whereas the E_0 value (2.147 eV) of the F8T2 polymer for at.200 μM was higher than the E_0 value (2.135 eV) of the F8T2 polymer at 2.290 μM. The α_c value of the F8T2 polymer sharply increased with increasing E and increasing molarity. The values of α_c at 1.200 and 2.290 μM were higher than those at 0.69 and 0.78, respectively. The propagation constants of the F8T2 polymer increased with increasing molarities. The ratio of the sq to sa value of the F8T2 film was found to be 1.271; this was reasonably close to the value predicted by theory. The F8T2 liquid-crystalline polymer had a high visible S at different molarities. The F8T2 polymer can be used in the fabrication of various sensors because of its good solubility, S, and response behavior.

ACKNOWLEDGMENTS

This work was supported by the Management Unit of the Scientific Research Projects of Muş Alparslan University under project 0001. The author is grateful to Hilal Gözler (R&D Scientist and Nanomagnetic Instruments Co.) for her help with the AFM measurements.

REFERENCES

1. Briseno, A. L.; Mannsfeld, S. C. B.; Jenekhe, S. A.; Bao, Z.; Xia, Y. *Mater. Today* **2008**, *11*, 38.
2. Gunduz, B.; Yakuphanoglu, F. *Sens. Actuators A* **2012**, *178*, 141.
3. Echabaane, M.; Rouis, A.; Bonnamour, I.; Ben Ouada, H. *Mater. Chem. Phys.* **2013**, *141*, 781.
4. Farag, A. A. M.; Osiris, W. G.; Ammar, A. H.; Mansour, A. M. *Synth. Met.* **2013**, *175*, 81.
5. Gunduz, B.; Yahia, I. S.; Yakuphanoglu, F. *Microelectron. Eng.* **2012**, *98*, 41.
6. Ameen, M. Y.; Abhijith, T.; Susmita, D.; Ray, S. K.; Reddy, V. S. *Org. Electron.* **2013**, *14*, 554.
7. Farag, A. A. M.; Gunduz, B.; Yakuphanoglu, F.; Farooq, W. A. *Synth. Met.* **2010**, *160*, 2559.
8. Graaf, H.; Schlettwein, D.; Jaeger, N. I. *Synth. Met.* **2000**, *109*, 151.
9. Kozma, E.; Catellani, M. *Dyes Pigments* **2013**, *98*, 160.
10. Lloyd, M. T.; Anthony, J. E.; Malliaras, G. G. *Mater. Today* **2007**, *10*, 34.
11. Zhang, Y. F.; Huang, L.; Sun, Y. B.; Han, B.; Cheng, H. S. *J. Cryst. Growth* **2013**, *374*, 79.
12. Zhu, Y.; Tour, J. M. *Nat. Photonics* **2012**, *6*, 72.
13. Gündüz, B. *Opt. Mater.* **2013**, *36*, 425.
14. Zhao, Y. S.; Fu, H.; Hu, F.; Peng, A. D.; Yao, *J. Adv. Mater.* **2007**, *19*, 3554.
15. Shirota, Y.; Kageyama, H. *Chem. Rev.* **2007**, *107*, 953.
16. Tseng, R. J.; Huang, J.; Ouyang, J.; Kaner, R. B.; Yang, Y. *Nano Lett.* **2005**, *5*, 1077.
17. Gunduz, B.; Al-Hartomy, O. A.; Al Said, S. A. F.; Al-Ghamdi, A. A.; Yakuphanoglu, F. *Synth. Met.* **2013**, *179*, 94.
18. Purniawan, A.; Pandraud, G.; Moh, T. S. Y.; Marthen, A.; Vakalopoulos, K. A.; French, P. J.; Sarro, P. M. *Sens. Actuators A* **2012**, *188*, 127.
19. Schmidt, R.; Ling, M. M.; Oh, J. H.; Winkler, M.; Könemann, M.; Bao, Z.; Würthner, F. *Adv. Mater.* **2007**, *19*, 3692.
20. Chen, Z.; Lee, M. J.; Ashraf, S.; Gu, R. Y.; Albert, S. S.; Nielsen, M. M.; Schroeder, B.; Anthopoulos, T. D.; Heeney, M.; McCulloch, I.; Sirringhaus, H. *Adv. Mater.* **2012**, *24*, 647.
21. Han, Y.; Wu, G.; Li, H.; Wang, W.; Chen, H. *Nanotechnology* **2010**, *21*, 185708.
22. Leclerc, M.; Najari, A. *Nat. Mater.* **2011**, *10*, 409.
23. Cerdan, L.; Costela, A.; Sampedro, G. D.; Moreno, I. G.; Calle, M.; Seva, M. J.; Abajo, J. D.; Turnbull, G. A. *J. Mater. Chem.* **2012**, *22*, 8938.
24. Carroll, D. O.; Lieberwirth, I.; Redmond, G. *Nat. Nanotechnol.* **2007**, *2*, 180.
25. Aziz, F.; Sayyad, M. H.; Sulaiman, K.; Mailis, B. Y.; Karimov, K. S.; Ahmad, Z.; Sugandi, G. *Meas. Sci. Technol.* **2012**, *23*, 014001.
26. Huang, Y.; Fu, L.; Zou, W.; Zhang, F.; Wei, Z. *J. Phys. Chem. C* **2011**, *115*, 10399.
27. Hu, J.; Kuang, W.; Deng, K.; Zou, W.; Huang, Y.; Wei, Z.; Faul, C. F. *J. Adv. Funct. Mater.* **2012**, *22*, 4149.
28. Rouis, A.; Dridi, C.; Dumazet-Bonnamour, I.; Davenas, J.; Ouada, H. B. *Phys. B* **2007**, *399*, 109.
29. Kajii, H.; Koiwai, K.; Hirose, Y.; Ohmori, Y. *Org. Electron.* **2010**, *11*, 509.
30. Werzer, O.; Matoy, K.; Smilgies, D. M.; Rothmann, M. M.; Strohriegl, P.; Resel, R. *J. Appl. Polym. Sci.* **2008**, *107*, 1817.
31. Huang, J. H.; Yang, C. Y.; Ho, Z. Y.; Kekuda, D.; Wu, M. C.; Chien, F. C.; Chen, P.; Chu, C. W.; Ho, K. C. *Org. Electron.* **2009**, *10*, 27.
32. Boucle, J.; Ravirajan, P.; Nelson, J. *J. Mater. Chem.* **2007**, *17*, 3141.
33. Ates, T.; Tatar, C.; Yakuphanoglu, F. *Sens. Actuators A* **2013**, *190*, 153.
34. Acar, H.; Karakışla, M.; Saçak, M. *J. Appl. Polym. Sci.* **2012**, *125*, 3977.
35. Peters, K. *Smart Mater. Struct.* **2011**, *20*, 013002.
36. Chen, X. J.; Zhang, J.; Ma, D. F.; Hui, S. C.; Liu, Y. L.; Yao, W. *J. Appl. Polym. Sci.* **2011**, *121*, 1685.
37. Sulaiman, K.; Ahmad, Z.; Fakir, M. S.; Wahab, F. A.; Abdullah, S. M.; Rahman, Z. A. *Mater. Sci. Forum* **2013**, *737*, 126.
38. Lilly, R. V.; Devaki, S. J.; Narayanan, R. K.; Sadanandhan, N. K. *J. Appl. Polym. Sci.* **2014**, *131*, 40936.
39. Lee, Y. S.; Joo, B. S.; Choi, N. J.; Lim, J. O.; Huh, J. S.; Lee, D. D. *Sens. Actuators B* **2003**, *93*, 148.
40. Pellegrino, T.; Kudera, S.; Liedl, T.; Javier, A. M.; Manna, L.; Parak, W. *J. Small* **2005**, *1*, 48.

41. El-Nahhas, M. M.; Abdel-Khalek, H.; Salem, E. *Adv. Cond. Matter Phys.* **2012**, *2012*, 698934.
42. Mitsushio, M.; Watanabe, K.; Abe, Y.; Higo, M. *Sens. Actuators A* **2010**, *163*, 1.
43. Lalova, A.; Todorov, R. *J. Phys. Conf. Ser.* **2012**, *398*, 012023.
44. Politakos, N.; Grana, E.; Zalakain, I.; Katsigiannopoulos, D.; Eceiza, A.; Kortaberria, G.; Avgeropoulos, A. *J. Appl. Polym. Sci.* **2014**, *131*, 40084.
45. Exley, J. R. Electrical and Optical Properties of Novel Phthalocyanine Compounds for Sensor Devices; Sheffield Hallam University: Sheffield, United Kingdom, **1995**.
46. Faisal, M.; Khan, S. B.; Rahman, M. M.; Jamal, A.; Umar, A. *Mater. Lett.* **2011**, *65*, 1400.
47. Rossberg, D. *Sens. Actuators A* **1996**, *54*, 793.
48. Armin, A.; Soltanolkotabi, M.; Feizollah, P. *Sens. Actuators A* **2011**, *165*, 181.
49. Manera, M. G.; Leo, G.; Curri, M. L.; Comparelli, R.; Rella, R.; Agostiano, A.; Vasanelli, L. *Sens. Actuators B* **2006**, *115*, 365.
50. Kumar, A.; Takashima, W.; Kaneto, K.; Prakash, R. *J. Appl. Polym. Sci.* **2014**, *131*, 40931.
51. Adhyapak, P.; Mahapure, P.; Aiyer, R.; Gosavi, S.; Mulik, U.; Amalnerkar, D. *J. Appl. Polym. Sci.* **2012**, *123*, 3565.
52. Abeles, F. Optical Properties of Solids; North-Holland: Amsterdam, **1972**.
53. Kaya, E.; Turan, N.; Gündüz, B.; Çolak, N.; Körkoca, H. *Polym. Eng. Sci.* **2012**, *52*, 1581.
54. Turan, N.; Kaya, E.; Gündüz, B.; Çolak, N.; Körkoca, H. *Fiber Polym.* **2012**, *13*, 415.
55. El-Nahass, M. M.; El-Gohary, Z.; Soliman, H. S. *Opt. Laser Technol.* **2003**, *35*, 523.
56. Wemple, S. H.; DiDomenico, M. *Phys. Rev. Lett.* **1969**, *23*, 1156.
57. Wemple, S. H.; DiDomenico, M. *Phys. Rev. B* **1971**, *3*, 1338.
58. Ali, A. I.; Son, J. Y.; Ammar, A. H.; Abdel Moez, A.; Kim, Y. S. *Results Phys.* **2013**, *3*, 167.
59. El-Nahhas, M.; Abdel-Khalek, H.; Salem, E. *Am. J. Mater. Sci.* **2012**, *2*, 131.
60. Veldhuis, G. J.; Parriaux, O.; Hoekstra, H. J. W. M.; Lambeck, P. V. *J. Lightw. Technol.* **2000**, *18*, 677.
61. Ward, H. C. In Rough Surfaces; Thomas, T. R., Ed.; Longman: London, **1982**; Chapter IV.
62. Kumar, B. R.; Rao, T. S. *Dig. J. Nanomater. Biostruct.* **2012**, *7*, 1881.
63. Gizli, N. *Chem. Chem. Technol.* **2011**, *5*, 327.
64. Kolanek, K.; Tallarida, M.; Karavaev, K.; Schmeisser, D. *Thin Solid Films* **2010**, *518*, 4688.
65. Feng, W.; Qi, Z.; Sun, Y. *J. Appl. Polym. Sci.* **2007**, *104*, 1169.